iScience

CellPress
OPEN ACCESS

Article

Monoacylglycerol acyltransferase-2 inhibits colorectal carcinogenesis in APC$^{min+/-}$ mice

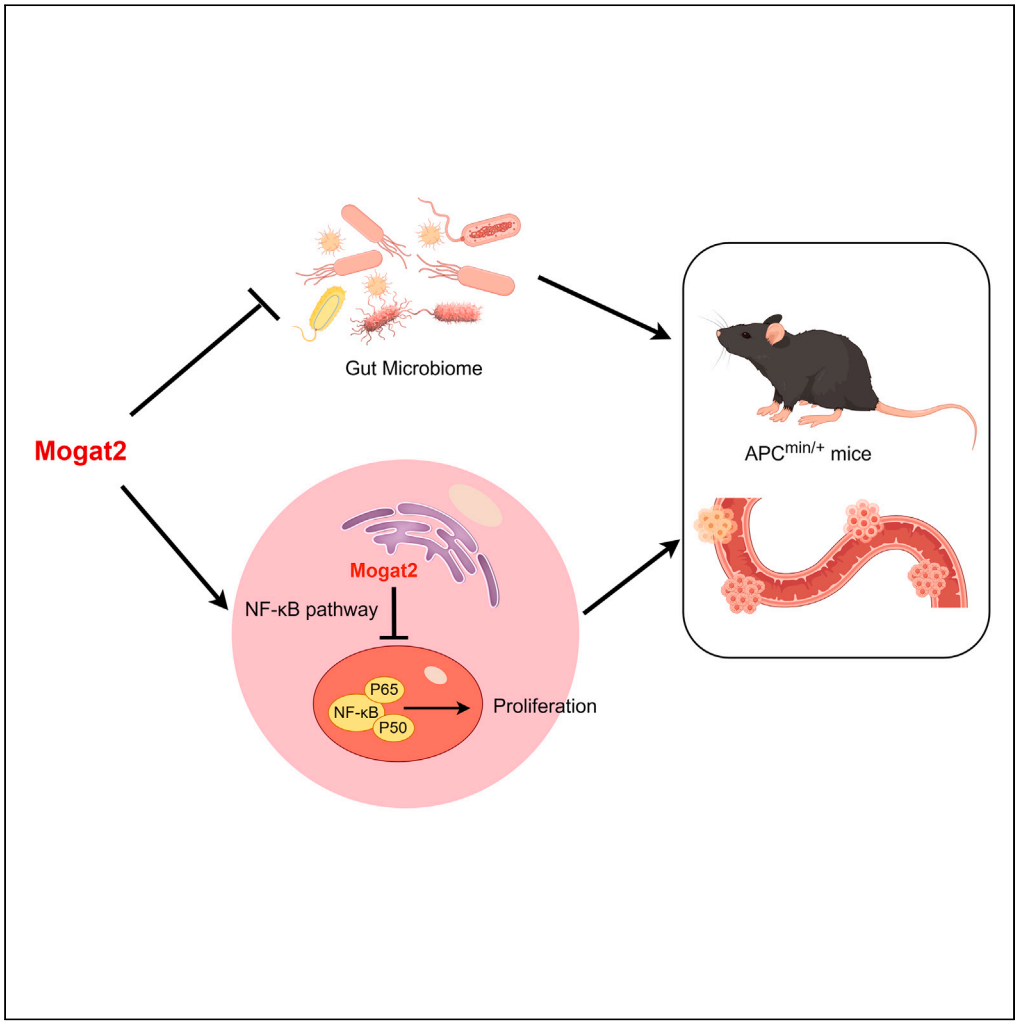

Yanhong Lang, Chengrui Zhong, Lingling Guo, ..., Yi Niu, Jiliang Qiu, Chaonan Qian

qiujl@sysucc.org.cn (J.Q.)
chaonan.qian@ccm.cn (C.Q.)

Highlights

Knocking out Mogat2 promotes intestinal tumor growth in Apc$^{Min/+}$ mice

Mogat2 knockout in mice alters the composition of gut microbiota

Gut microbiota from Mogat2$^{-/-}$ mice promotes intestinal tumor growth

Mogat2 suppresses colorectal cancer cell proliferation by the NF-κB signaling pathway

Lang et al., iScience 27, 110205
July 19, 2024
https://doi.org/10.1016/j.isci.2024.110205

iScience

CellPress
OPEN ACCESS

Article

Monoacylglycerol acyltransferase-2 inhibits colorectal carcinogenesis in APC$^{min+/-}$ mice

Yanhong Lang,[1,2] Chengrui Zhong,[1] Lingling Guo,[1] Zhijie Liu,[1] Dinglan Zuo,[1] Xi Chen,[1] Liuyan Ding,[1] Bijun Huang,[1] Binkui Li,[1,2] Yunfei Yuan,[1,2] Yi Niu,[1] Jiliang Qiu,[1,2,4,5,*] and Chaonan Qian[1,3,4,*]

SUMMARY

Monoacylglycerol acyltransferase-2 (MOGAT2), encodes MOGAT enzyme in the re-synthesis of triacylglycerol and protects from metabolism disorders. While, its precise involvement in colorectal cancer (CRC) progression remains inadequately understood. Our study demonstrated that knockout of Mogat2 in Apc$^{min/+}$ mice expedited intestinal tumor growth and progression, indicating that Mogat2 plays a tumor-suppressing role in CRC. Mechanically, Mogat2 deletion resulted in a significant alter the gut microbiota, while Fecal Microbiota Transplantation (FMT) experiments demonstrated that the gut microbiota in Mogat2 deleted mice promoted tumor growth. Furthermore, we identified Mogat2 as a functional regulator suppressing CRC cell proliferation and tumor growth by inhibiting the NF-κB signaling pathway *in vivo*. Collectively, these results provide novel insights into the protective double roles of Mogat2, inhibiting of NF-κB pathway and keeping gut microbiota homeostasis in colorectal cancer, which may help the development of novel cancer treatments for CRC.

INTRODUCTION

Colorectal cancer (CRC) is one of the major malignancies and accounts for approximately 9% of all cancer cases.[1,2] Approximately 80% of patients with colorectal cancer have inactivating mutations in the adenomatous polyposis coli (APC) tumor suppressor gene, which acts as a negative regulator of canonical Wnt signaling.[3] CRC involves a complex mechanism of carcinogenesis, encompassing various risk factors for its initiation, promotion, progression, relapse, and metastasis. These factors include environmental elements such as obesity, being of an older age, male gender, lifestyle, physical inactivity, smoking, and genetic predisposition.[4–6] Despite great efforts in researching CRC carcinogenesis, the detailed molecular mechanisms have not been fully elucidated.

Perturbed fat metabolism has been found to be critical in many biological steps regulating tumor initiation and progression.[7,8] Increasing evidence has investigated the role of the fat metabolism in cancer.[9–12] Triacylglycerol (TAG) is a major source of calories, which can be hydrolyzed to monoacylglycerols (MAG) and fatty acids (FA) in the small intestinal lumen. The hydrolysis products are then resynthesized into TAG in enterocytes via two pathways: the glycerol-3-phosphate pathway and the MAG pathway, which accounts for approximately 75% of TAG resynthesis.[13–15] Mogat2 is a member of the DGAT2 family, which is highly expressed in the endoplasmic reticulum of enterocytes in the small intestine. Its function is to catalyze the conversion of MAG to DAG, which is the first step in TAG production.[16–18] It has been reported that Mogat2-deficient mice prevent high-fat diet-induced obesity, glucose intolerance, hypercholesterolemia, and fatty liver.[13,16,19,20] However, the function of Mogat2 remains poorly characterized in colorectal cancer progression, and its pathological significance needs to be determined.

In this study, we observed that knockout of Mogat2 in the Apc$^{min/+}$ spontaneous intestinal adenoma mice model enhanced intestinal adenoma progression and reduced the survival time of the mice. We also discovered significant differences in intestinal microbial communities between C57BL/6J (WT) and Mogat2$^{-/-}$ mice; Apc$^{min/+}$ mice and Apc$^{Min/+}$; Mogat2$^{-/-}$ mice. FMT experiments also suggested that the fecal samples of Mogat2$^{-/-}$ mice can accelerate intestinal tumorigenesis in Apc$^{min/+}$ mice. Furthermore, we found that overexpression of Mogat2 in CRC cells can inhibit cellular proliferation and tumor growth by NF-κB pathway *in vivo*. These findings identify a protective role of Mogat2 in colorectal cancer, extending our current understanding beyond its role in fat metabolism regulation.

[1]State Key Laboratory of Oncology in South China, Guangdong Provincial Clinical Research Center for Cancer, Sun Yat-Sen University Cancer Center, Guangzhou 510060, P.R. China
[2]Department of Liver Surgery, Sun Yat-sen University Cancer Center, 651 Dongfeng Road East, Guangzhou 510060, P.R. China
[3]Department of Radiation Oncology, Guangzhou Concord Cancer Center, 9 Ciji Road, Huangpu District, Guangzhou 510555, P.R. China
[4]These authors contributed equally
[5]Lead contact
*Correspondence: qiujl@sysucc.org.cn (J.Q.), chaonan.qian@ccm.cn (C.Q.)
https://doi.org/10.1016/j.isci.2024.110205

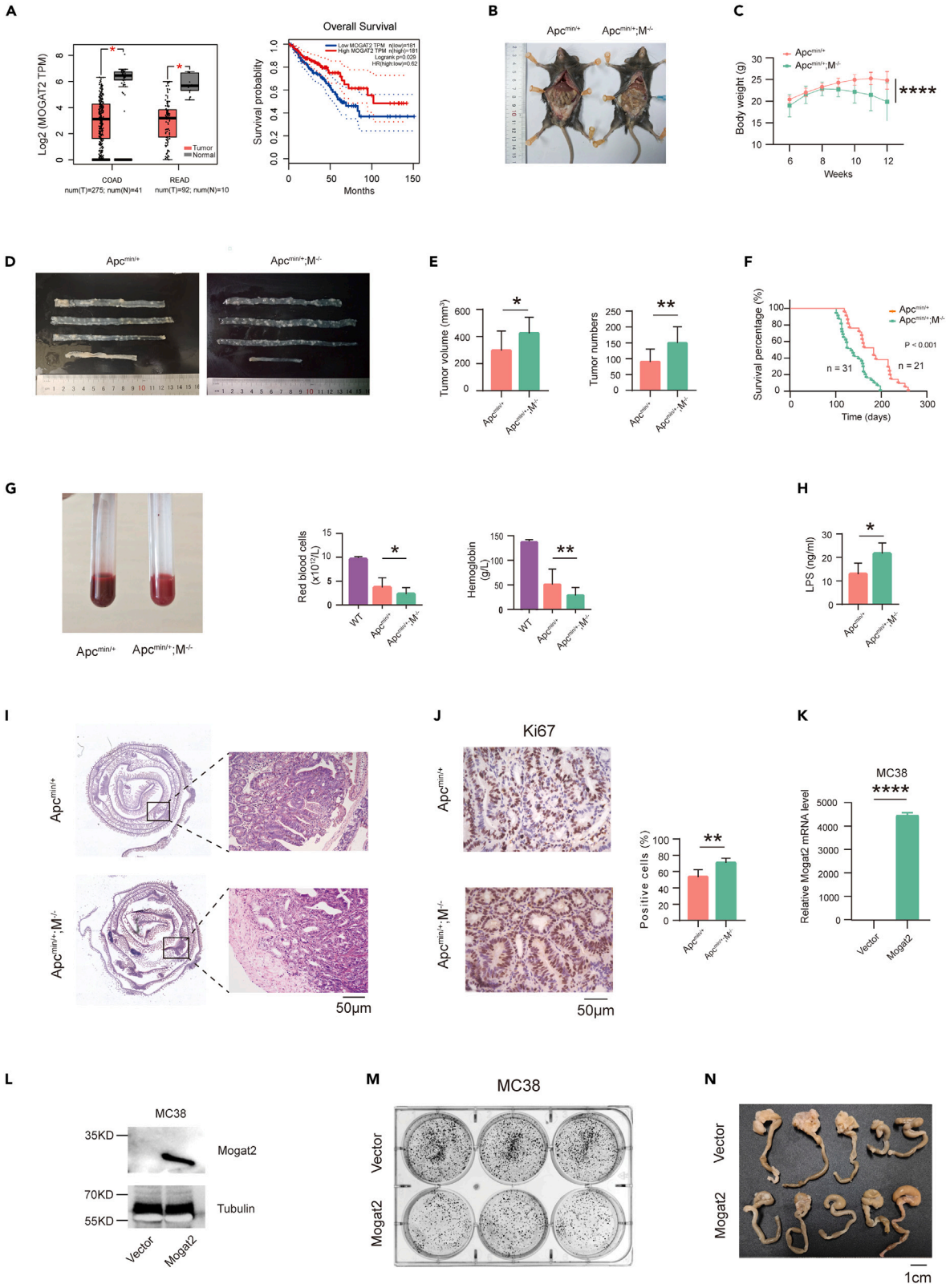
A
Log2 (MOGAT2 TPM)
Tumor
Normal
COAD
num(T)=275; num(N)=41
READ
num(T)=92; num(N)=10
Overall Survival
Survival probability
Months
B
Apc^min/+
Apc^min/+;M^-/-
C
Body weight (g)
Weeks
****
D
Apc^min/+
Apc^min/+;M^-/-
E
Tumor volume (mm^3)
Tumor numbers
F
Survival percentage (%)
Time (days)
P < 0.001
n = 31
n = 21
G
Apc^min/+
Apc^min/+;M^-/-
Red blood cells (x10^12/L)
Hemoglobin (g/L)
WT
H
LPS (ng/ml)
I
50μm
J
Ki67
Positive cells (%)
50μm
K
MC38
Relative Mogat2 mRNA level
Vector
Mogat2
L
MC38
35KD
70KD
55KD
Mogat2
Tubulin
Vector
Mogat2
M
MC38
Vector
Mogat2
N
Vector
Mogat2
1cm

Figure 1. Deletion of Mogat2 promotes tumorigenesis in $Apc^{Min/+}$ mice

(A) The mRNA level of Mogat2 in cancer tissues and non-cancerous tissues from the GEPIA database (left) and Kaplan-Meier analysis of the overall survival of patients with CRC with high or low Mogat2 expression from the GEPIA database (right).

(B) Representative dissecting gross image of $Apc^{Min/+}$ and $Apc^{Min/+}$; $Mogat2^{-/-}$ mice.

(C) Body weight of the $Apc^{Min/+}$ (n = 8) and $Apc^{Min/+}$; $Mogat2^{-/-}$ mice (n = 10)

(D) Representative dissecting gross image of small intestines and colons from the $Apc^{Min/+}$ and $Apc^{Min/+}$; $Mogat2^{-/-}$ mice.

(E) Total number and volume of tumors of the $Apc^{Min/+}$ (n = 13) and $Apc^{Min/+}$; $Moagt2^{-/-}$ mice (n = 10) in the small intestine mice calculated according to the diameter.

(F) Kaplan-Meier plot analysis of the survival of $APC^{Min/+}$ (n = 31) and $Apc^{Min/+}$; $Mogat2^{-/-}$ (n = 21) mice.

(G) Representative blood image of $Apc^{Min/+}$ and $Apc^{Min/+}$; $Mogat2^{-/-}$ mice. The number of red blood cells and the concentration of hemoglobin in $Apc^{Min/+}$ (n = 16) and $Apc^{Min/+}$; $Mogat2^{-/-}$ mice (n = 22).

(H) The level of LPS in the serum of $Apc^{Min/+}$ (n = 5) and $Apc^{Min/+}$; $Mogat2^{-/-}$ mice (n = 5).

(I) H&E staining of the intestines from the $Apc^{Min/+}$ mice and $Apc^{Min/+}$; $Moagt2^{-/-}$ mice, five views were randomly selected from each section to calculate the percentage of positive cells per crypt.

(J) Immunohistochemical staining for Ki67 in the intestinal tumor tissues from $Apc^{Min/+}$ and $Apc^{Min/+}$; $Moagt2^{-/-}$ mice, five views were randomly selected from each section to calculate the percentage of positive cells per crypt.

(K) Quantitative PCR analysis of Mogat2 mRNA level in the MC38 overexpressing cells. Mogat2 mRNA level was normalized to β-actin, Column, mean; bar, s.d. (from triplicates).

(L) Immunoblotting analysis of Mogat2 protein levels in the MC38 overexpressing cells and MC38 vector cells. Alpha-tubulin was used as the loading control.

(M) Image of the colony formation assay of the MC38 cells with or without Mogat2 overexpression.

(N) Representative images showing primary tumors in cecum. Significance was established by unpaired t test (E, G, H, J, K) and two-way ANOVA (D). *$p < 0.05$, **$p < 0.01$, ***$p < 0.001$, ****$p < 0.0001$.

RESULTS

Knock out of monoacylglycerol acyltransferase-2 promotes intestinal tumor growth in $Apc^{Min/+}$ mice

To investigate the clinical significance of Mogat2 in colorectal cancer, we initially analyzed the expression levels of Mogat2 using the Gene Expression Profiling Interactive Analysis (GEPIA) tool (http://gepia.cancer-pku.cn/). Analysis of the GEPIA database indicated a significant decrease in Mogat2 expression levels in tumor specimens from patients with Colon Adenocarcinoma and Rectum Adenocarcinoma (CRC) compared to normal colon tissues (Figure 1A, left). We further found that MOGAT2 expression was positively correlated with overall survival in patients with CRC (Figure 1A, right). To explore the role of Mogat2 in tumorigenesis, we generated $Apc^{Min/+}$; $Mogat2^{-/-}$ mice by crossing $Apc^{Min/+}$ mice with $Mogat2^{-/-}$ mice (Figure 1B). Our experiments revealed that $Apc^{Min/+}$; $Mogat2^{-/-}$ mice exhibited significant weight loss compared to $Apc^{Min/+}$ mice (Figure 1C). After excising the small intestines from 16-week-old $Apc^{Min/+}$ and $Apc^{Min/+}$; $Mogat2^{-/-}$ mice, we counted the intestinal tumors with a stereoscopic microscope to detect differences in tumor growth. The $Apc^{Min/+}$; $Mogat2^{-/-}$ mice had a higher mean volume, a greater number of small intestine tumors, (Figures 1D and 1E) and a shorter survival time compared to the $Apc^{Min/+}$ mice (Figure 1F), indicating that Mogat2 deletion promotes intestinal tumorigenesis. Furthermore, the pictures of hematoxylin-eosin staining show many tumor cells invading the basement membrane of the small intestine in $Apc^{Min/+}$; $Mogat2^{-/-}$ mice, but there is no tumor cells invading the basement membrane of the small intestine in $Apc^{Min/+}$ mice (Figure 1I), it showed severe malignant tumor progression in $Apc^{Min/+}$; $Mogat2^{-/-}$ mice.

Additionally, we examined the red blood cells and hemoglobin levels of $Apc^{Min/+}$ mice and found that $Apc^{Min/+}$; $Mogat2^{-/-}$ mice had decreased levels of both red blood cells and hemoglobin (Figure 1G). Intestinal barrier dysfunction can aggravate the development of colitis and CRC, we detect the Lipopolysaccharide (LPS) in the serum of mice, we also found a higher serum level of LPS in $Apc^{Min/+}$; $Mogat2^{-/-}$ mice than $Apc^{Min/+}$ mice (Figure 1H). This finding suggests that the $Apc^{Min/+}$; $Mogat2^{-/-}$ mice display more severe anemic conditions. Nonetheless, metastasis to the liver was absent in both groups (Figure S1A).

By utilizing Ki-67 expression to quantify the proliferating cells within the polyps, we noted a greater proportion of proliferating cells in the polyps of $Apc^{Min/+}$; $Mogat2^{-/-}$ mice (see Figure 1J). It is important to highlight that no disparities were observed in the counts of white blood cells including monocytes, lymphocytes, and neutrophils, nor platelets within the blood (Figure S1B).

MC38 is a tumorigenic yet poorly metastatic mouse colon cancer cell line. To explore the effects of Mogat2, we generated MC38 cells with stable overexpression of Mogat2. The overexpression of Mogat2 was confirmed using real-time quantitative PCR and western blotting (Figures 1K and 1L). Further, colony formation assays demonstrated that Mogat2 overexpression inhibited tumor growth (Figure 1M). To investigate the progression of CRC in response to Mogat2 overexpression, we employed a orthotopic mouse model. This involved injecting either MC38 cells with a vector control or MC38 cells overexpressing Mogat2 into the cecum of syngeneic C57BL/6J mice. MC38-vector cells led to the formation of three tumors in five mice. In contrast, fewer tumor was observed in mice injected with Mogat2-overexpressing MC38 cells (Figure 1N). Therefore, Mogat2 overexpression in MC38 cells significantly inhibited tumor incidence and growth.

Loss of monoacylglycerol acyltransferase-2 significantly alters the composition of gut microbiota in wild type mice

To better understand the effect of Mogat2 on gut microbiota, we performed 16S rRNA gene sequencing of fecal samples from WT mice and $Mogat2^{-/-}$ mice. Beta-diversity analysis, utilizing principal coordinate analysis, showed a notable separation between the two groups (Figure 2A). A Venn diagram identified 95 overlapping operational taxonomic units (OTUs), with 3 OTUs specific to the WT group and 5 OTUs

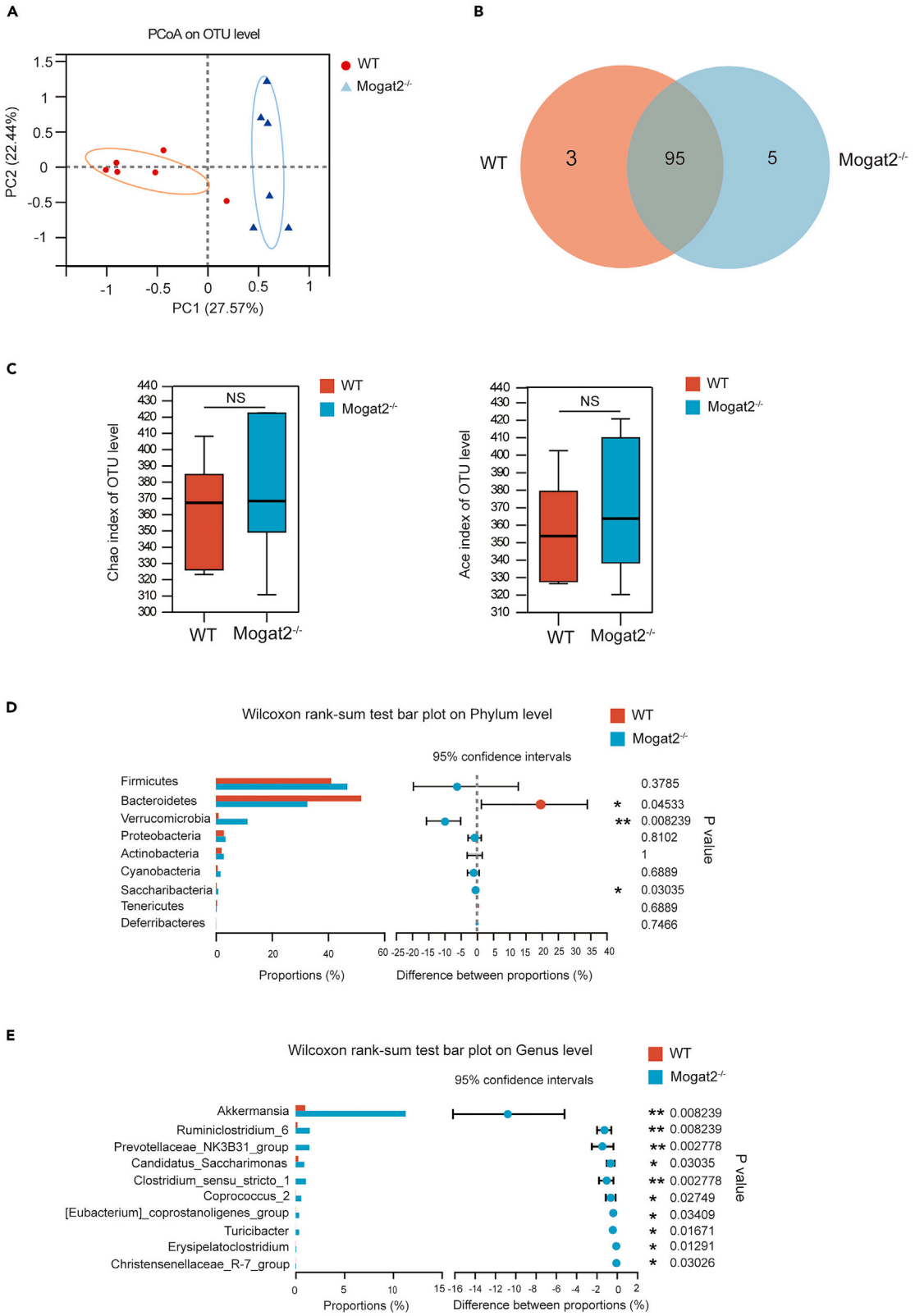
A
PCoA on OTU level
WT
Mogat2-/-
PC2 (22.44%)
PC1 (27.57%)
B
WT
3
95
5
Mogat2-/-
C
Chao index of OTU level
NS
WT
Mogat2-/-
Ace index of OTU level
NS
WT
Mogat2-/-
D
Wilcoxon rank-sum test bar plot on Phylum level
95% confidence intervals
Firmicutes
Bacteroidetes
Verrucomicrobia
Proteobacteria
Actinobacteria
Cyanobacteria
Saccharibacteria
Tenericutes
Deferribacteres
0.3785
* 0.04533
** 0.008239
0.8102
1
0.6889
* 0.03035
0.6889
0.7466
P value
Proportions (%)
Difference between proportions (%)
E
Wilcoxon rank-sum test bar plot on Genus level
95% confidence intervals
Akkermansia
Ruminiclostridium_6
Prevotellaceae_NK3B31_group
Candidatus_Saccharimonas
Clostridium_sensu_stricto_1
Coprococcus_2
[Eubacterium]_coprostanoligenes_group
Turicibacter
Erysipelatoclostridium
Christensenellaceae_R-7_group
** 0.008239
** 0.008239
** 0.002778
* 0.03035
** 0.002778
* 0.02749
* 0.03409
* 0.01671
* 0.01291
* 0.03026
P value
Proportions (%)
Difference between proportions (%)

Figure 2. Alterations in Microbiota Dysbiosis Observed in Mogat2$^{-/-}$ mice

(A) Principle coordination analysis (PCoA) was performed based on OTU abundance.

(B) Venn diagram analysis compared the fecal samples of WT mice and Mogat2$^{-/-}$ mice.

(C) Alpha-diversity analysis using the Chao and Ace indexes to compare the community richness between the two groups.

(D) The taxonomic composition distribution at the phylum level of fecal microbiota was compared between the two groups.

(E) The taxonomic composition distribution at the genus level of fecal microbiota was compared between the two groups (6 mice per group). ***$p < 0.001$, **$p < 0.01$, *$p < 0.05$.

exclusive to the Mogat2$^{-/-}$ group (Figure 2B). When assessing community richness through alpha-diversity using the Chao and Ace indices, no statistically significant difference was observed between the groups ($p = 0.64$, $p = 0.557$) (Figure 2C). An analysis of the gut microbiota composition at the phylum level revealed that Mogat2 deficiency decreased the relative abundance of Bacteroidetes (51.8% in the WT vs. 32.6% in the Mogat2$^{-/-}$, $p < 0.05$), while increasing the relative abundance of Saccharibacteria (0.27% in the WT vs. 0.89% in the Mogat2$^{-/-}$, $p < 0.05$) and Verrucomicrobia (0.98% in the WT vs. 11.3% in the Mogat2$^{-/-}$, $p < 0.05$) (Figure 2D). Comparative analysis at the microbial genus level revealed that Mogat2 deficiency significantly elevated the abundance of several genera, including *Akkermansia*, *Ruminiclostridium_6*, *Prevotellaceae_NK3B31_group*, and *Clostridium_sensu_stricto_1* (Figure 2E). Collectively, these findings underscore the pivotal role of Mogat2 in regulating the composition of gut microbiota in mice.

Loss of monoacylglycerol acyltransferase-2 alters the composition of gut microbiota in Apc$^{Min/+}$ mice

To further investigate whether Mogat2 knockout affects the gut microbiota during CRC, we analyzed the microbial composition of the Apc$^{Min/+}$ mice and Apc$^{Min/+}$; Mogat2$^{-/-}$ mice. The PCoA analysis demonstrated a significant separation between the two groups (Figure 3A). Venn diagram analysis revealed that 96 OTUs were shared between the groups, while 6 OTUs were present only in the Apc$^{Min/+}$ mice group, and 14 OTUs were present specific in the Apc$^{Min/+}$; Mogat2$^{-/-}$ group (Figure 3B). The quantification of microbial diversity via the Chao and Ace diversity indexes showed significant differences between the two groups (p=0.0065 and p=0.0016), respectively (Figure 3C).

Compared to Apc$^{Min/+}$ mice, the Apc$^{Min/+}$; Mogat2$^{-/-}$ mice exhibited a significant alteration in their microbial composition. Specifically, the Apc$^{Min/+}$; Mogat2$^{-/-}$ mice showed a significant increase in the abundance of Verrucomicrobia (0.03% vs. 3.24%, $p < 0.01$) and Actinobacterio (0.04% vs. 0.15%, $p < 0.05$) phyla compared to Apc$^{Min/+}$ mice, while the proportion of the Deferribacteres phylum was markedly decreased (0.68% vs. 0.04%, $p < 0.05$) in the Apc$^{Min/+}$; Mogat2$^{-/-}$ mice (Figure 3D). At the genus level, Apc$^{Min/+}$; Mogat2$^{-/-}$ mice exhibited a significant increase in *Akkermansia* (3.25%) compared to Apc$^{Min/+}$ mice (0.03%) ($p < 0.05$). Additionally, other genera, such as *Bacteroides*, *Prevotellaeae_NK3B31_group*, and *Clostridium_sensu_stricto_1*, also increased in abundance in the Apc$^{Min/+}$; Mogat2$^{-/-}$ mice (Figure 3E).

Gut microbiota from monoacylglycerol acyltransferase-2 knockout -mice aggravates the progression of intestinal adenoma

To evaluate the impact of gut microbiota derived from Mogat2$^{-/-}$ mice on intestinal adenoma in 16-week-old Apc$^{Min/+}$ mice, pseudo-germ-free (PGF) mice and FMT was conducted (Figures 4A and 4B). A higher total adenoma count was observed in Apc$^{Min/+}$ mice that received fecal samples from Mogat2$^{-/-}$ mice, compared to those that received fecal samples from WT mice, indicating that the gut microbiota from Mogat2$^{-/-}$ mice promoted the progression of intestinal adenoma in Apc$^{Min/+}$ mice (Figure 4C). Furthermore, the rate of Ki-67-positive cells in the FMT-Mogat2 group was significantly higher than in the FMT-WT group (Figure 4D). Moreover, the goblet cells play an important role in maintaining intestinal health during steady-state, we found the average number of goblet cells in each crypt was significantly lower in the FMT-Mogat2 group than in the FMT-WT group (Figure 4E). These results suggest that gut microbiota from Mogat2$^{-/-}$ mice could promote the proliferation of intestinal tumor cells.

Overexpression of monoacylglycerol acyltransferase-2 inhibits colorectal cancer cell growth *in vitro* and *in vivo*

The Mogat2 protein expression levels were examined in seven CRC cell lines. Western blot assays showed that Mogat2 had low expression in SW620 and HT29 cells (Figure 5A). To further investigate the role of Mogat2 in CRC development, Mogat2 was stably overexpressed in the human CRC cell lines HT29 and SW620, and the overexpression of Mogat2 was confirmed by real-time quantitative PCR and western blotting (Figures 5B and 5C). Overexpression of Mogat2 reduced the proliferation markers FoxM1 and MYC, as confirmed by Q-PCR (Figure 5D), and inhibited cell proliferation and colony formation, as evidenced by CCK8 and colony formation assays (Figures 5E and 5F). To validate the function of Mogat2 *in vivo*, 4×10^6 SW620 cells and Mogat2-overexpressing SW620 cells were subcutaneously injected into the dorsal flank of nude mice, and the tumor sizes were measured 17 days later (Figure 5G). The results showed that Mogat2-overexpressing cells significantly decreased tumor volume and weight, suggesting that Mogat2 acts as a tumor suppressor in CRC. To further reveal the molecular mechanism by which Mogat2 inhibits the progression of CRC, RNA-seq analysis was performed on SW620 cells transfected with control and overexpression for Mogat2. The results showed that 70 genes were up-regulated and 131 genes were down-regulated in Mogat2-overexpressing SW620 cells compared with SW620 vector cells (Figure 5H). Kyoto Encyclopedia of Genes and Genomes (KEGG) pathway enrichment analysis revealed that Mogat2 regulates the NF-κB pathway (Figure 5I). We then detected the protein level of P65, p-P65, P50, IKBα, and *p*-IKBα in vector and overexpression cell lines. The P65, p-P65, P50, and *p*-IKBα protein levels were decreased and IKBα was increased in Mogat2 overexpressing cells (Figure 5J), these results revealed that Mogat2 could inhibit the NF-κB signaling activation.

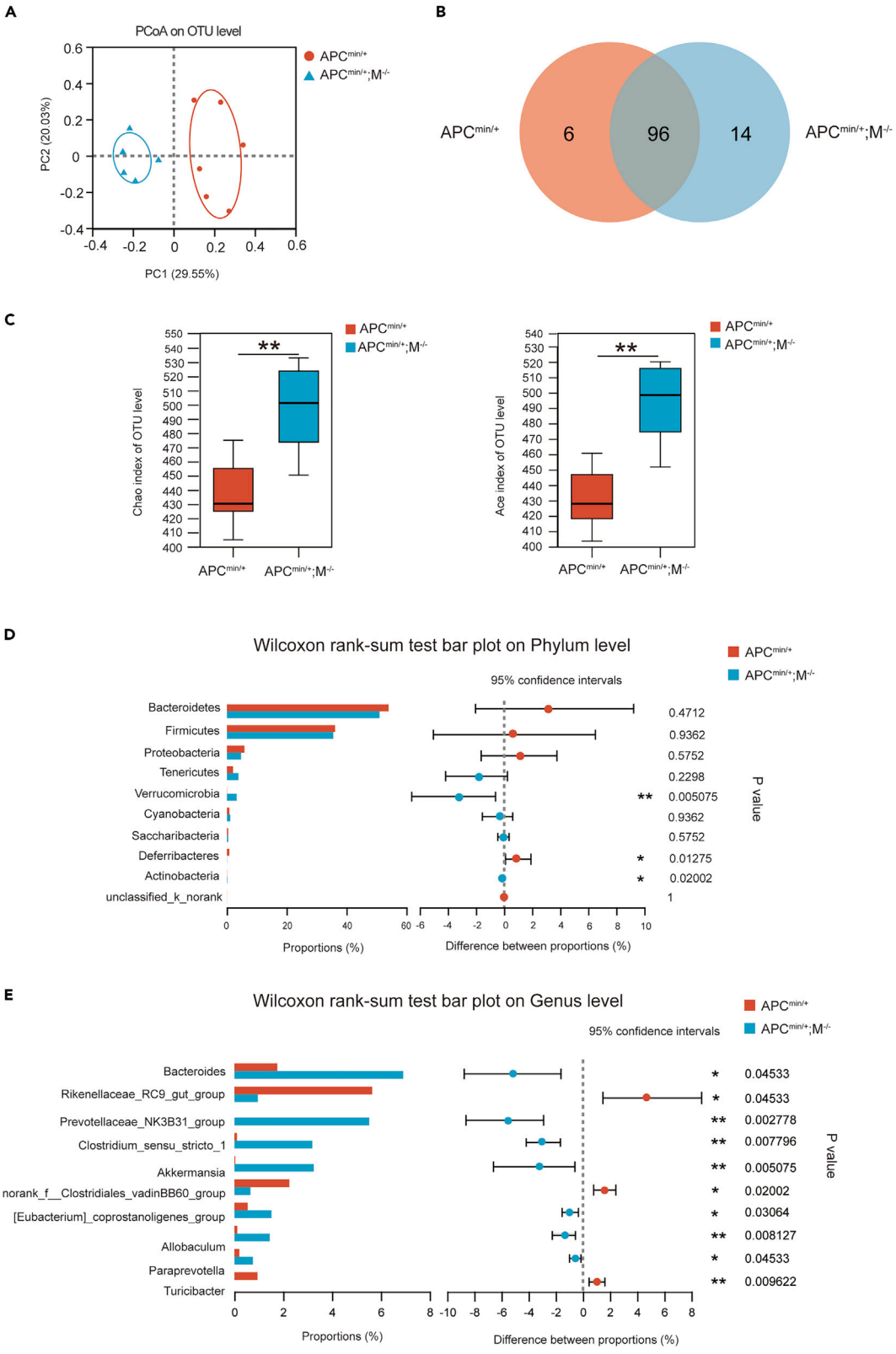
A
PCoA on OTU level
APCmin/+
APCmin/+;M-/-
PC2 (20.03%)
PC1 (29.55%)
B
APCmin/+
6
96
14
APCmin/+;M-/-
C
Chao index of OTU level
Ace index of OTU level
**
APCmin/+
APCmin/+;M-/-
D
Wilcoxon rank-sum test bar plot on Phylum level
95% confidence intervals
Bacteroidetes
Firmicutes
Proteobacteria
Tenericutes
Verrucomicrobia
Cyanobacteria
Saccharibacteria
Deferribacteres
Actinobacteria
unclassified_k_norank
0.4712
0.9362
0.5752
0.2298
** 0.005075
0.9362
0.5752
* 0.01275
* 0.02002
1
P value
Proportions (%)
Difference between proportions (%)
E
Wilcoxon rank-sum test bar plot on Genus level
95% confidence intervals
Bacteroides
Rikenellaceae_RC9_gut_group
Prevotellaceae_NK3B31_group
Clostridium_sensu_stricto_1
Akkermansia
norank_f__Clostridiales_vadinBB60_group
[Eubacterium]_coprostanoligenes_group
Allobaculum
Paraprevotella
Turicibacter
* 0.04533
* 0.04533
** 0.002778
** 0.007796
** 0.005075
* 0.02002
* 0.03064
** 0.008127
* 0.04533
** 0.009622
P value
Proportions (%)
Difference between proportions (%)

Figure 3. Microbiota dysbiosis alterations in Apc$^{Min/+}$ mice with Mogat2 deletion

(A) Principle coordination analysis (PCoA) based on OTU abundance.

(B) Venn diagram analysis of fecal samples from Apc$^{Min/+}$ and Apc$^{Min/+}$; Mogat2$^{-/-}$ mice.

(C) Alpha-diversity comparison between two groups using Chao and Ace indexes.

(D) The taxonomic composition distribution among the two groups on the phylum-level of the fecal microbiota.

(E) The taxonomic composition distribution among the two groups at the genus-level of the fecal microbiota. (6 mice per group). ***$p < 0.001$, **$p < 0.01$, *$p < 0.05$.

DISCUSSION

The Apc$^{Min/+}$ mouse model carries a mutation at codon 850 of the human Apc gene, resulting in the constitutive activation of Wnt signaling in the intestine.[21] Due to the mutation in multiple intestinal neoplasia, Apc$^{Min/+}$ mice spontaneously develop multiple adenomatous polyps in the small intestine and fewer polyps in the colon.[22,23] Therefore, Apc$^{Min/+}$ mice remain a classic mouse model for studying human intestinal tumorigenesis.[24–27] The Apc$^{Min/+}$; Mogat2$^{-/-}$ mice model was established to investigate the effect of Mogat2 on spontaneous intestinal adenocarcinoma in mice with an APC mutation. Our study revealed that the number and volume of intestinal tumors significantly increased after knocking out Mogat2, along with an accelerated pathological progression of the tumors in Apc$^{Min/+}$; Mogat2$^{-/-}$ mice. To sum up, our studies highlight the inhibiting roles of Mogat2 in CRC.

The gut microbiome is recognized as a mediating factor that contributes to the connection between environmental factors and the development of colorectal cancer.[28–31] In recent decades, increasing evidence has shown that the gut microbiota plays a pivotal role in the carcinogenic process.[32] Microbiota has been implicated in around 20% of cancers, particularly CRC.[33–35] The human gut microbiota is predominantly categorized into three major phyla: Firmicutes (30%–50%), Bacteroidetes (20%–40%), and Actinobacteria (1%–10%). Notably, alterations at the phylum level, including an increase in Bacteroidetes and a decrease in Firmicutes and Proteobacteria, have been reported in relation to colorectal cancer incidence.[33]

In our study, we observed that the loss of Mogat2 did not result in alterations in the abundance of Bacteroidetes, Firmicutes, and Proteobacteria in Apc$^{Min/+}$ mice. However, the loss of Mogat2 led to an increase in Verrucomicrobia at the phylum level and a heightened presence of *Akkermansia muciniphila* at the genus level. *Akkermansia muciniphila*, a gram-negative anaerobic bacterium, is one of the most prevalent species within the human gut microbiota, constituting1 to 5% of the microbial population in the human intestine and is the only known member of the Verrucomicrobia phylum found in the human intestinal tract.[36,37] *Akkermansia muciniphila* has recently been identified as a promising probiotic candidate.[37,38] Importantly, it is worth noting that the abundance of *Akkermansia muciniphila* is significantly lower in individuals with metabolic disorders including diabetes and obesity.[38]

However, there are studies that have demonstrated a significant decrease in the mRNA and protein expression levels of tight junction proteins in the over-colonized *Akkermansia muciniphila* mouse model.[39,40] Qin's group revealed that the excessive colonization of *Akkermansia muciniphila* disrupts the delicate equilibrium between mucin secretion and degradation. This disruption leads to a thinning of the intestinal mucous layer and compromises the integrity of the intestinal barrier. As a consequence, this situation can aggravate the development of colitis and CRC.[40] Previous investigations into *Akkermansia muciniphila* have established its status as a beneficial bacterium that plays a crucial role in maintaining intestinal homeostasis.[41] Treatment with *Akkermansia muciniphila* has been shown to reverse metabolic disorders induced by a high-fat diet, effectively countering issues such as increased fat mass, metabolic endotoxemia, adipose tissue inflammation, and insulin resistance.[41] However, excessive colonization of *Akkermansia muciniphila* disrupts the balance between mucin secretion and degradation, leading to damage to the intestinal barrier. Ultimately, this disruption exacerbates the development of colitis and colorectal cancer.[40] In the present study, the deletion of Mogat2 was also found to increase the abundance of *Clostridium_sensu_stricto_1*. *Clostridium_sensu_stricto_1* has been reported to exhibit a significant association with colon inflammation and the integrity of the intestinal barrier. This association is indicated by a positive correlation between the mRNA expression of colonic TLR4, TLR5, and NF-κB.[39] To further investigate the role of the gut microbiota in adenoma progression, fecal microbiota transplantation was performed.[42] This transplantation indicated that the gut microbiota from Mogat2$^{-/-}$ mice could promote the development of intestinal adenomas.

NF-κB has been widely implicated in the development and progression of cancer.[43] NF-κB acts as a collective term for a family NF-κB of five related Rel proteins: RelA/p65, c-Rel, RelB, NF-κB1 (also known as p50, p105 or p50/p105) and NF-κB 2 (also known as p52, p100 or p52/100). In colorectal cancer, NF-κB plays a critical role in cell proliferation, apoptosis, angiogenesis, and metastasis.[44,45] In order to investigate the role of Mogat2 in CRC progression *in vivo*, we constructed cell lines with stable overexpression of Mogat2 in HT29 and SW620 cells. Our experiments revealed that Mogat2 overexpression inhibited cellular proliferation and colony formation. The interaction of Mogat2 and NF-κB pathway was not reported in the previous study. In the present study, we found that P65, p-P65, P50, and *p*-IKBα, key factors in the NF-κB pathway, were decreased when overexpression of Mogat2. The findings of this study highlight that the overexpression of Mogat2 could inhibit the NF-κB pathway in CRC cells.

Previous studies have considered Mogat2 as an intervention target to address obesity and related metabolic diseases.[20,46,47] However, our findings reveal that Mogat2 assumes a tumor-suppressive role in the formation of intestinal tumors: directly inhibit CRC cells growth via NF-κB pathway, as well keep the gut microbiota homeostasis. Loss of Mogat2 not only accelerates intestinal tumor growth but also expedites the pathological processes involved. The disrupted gut microbiota observed in Mogat2$^{-/-}$ mice further enhances the advancement of intestinal adenomas in Apc$^{min/+}$ mice. These results offer new perspectives to understand cancer development and novel strategies for potential target therapy for CRC.

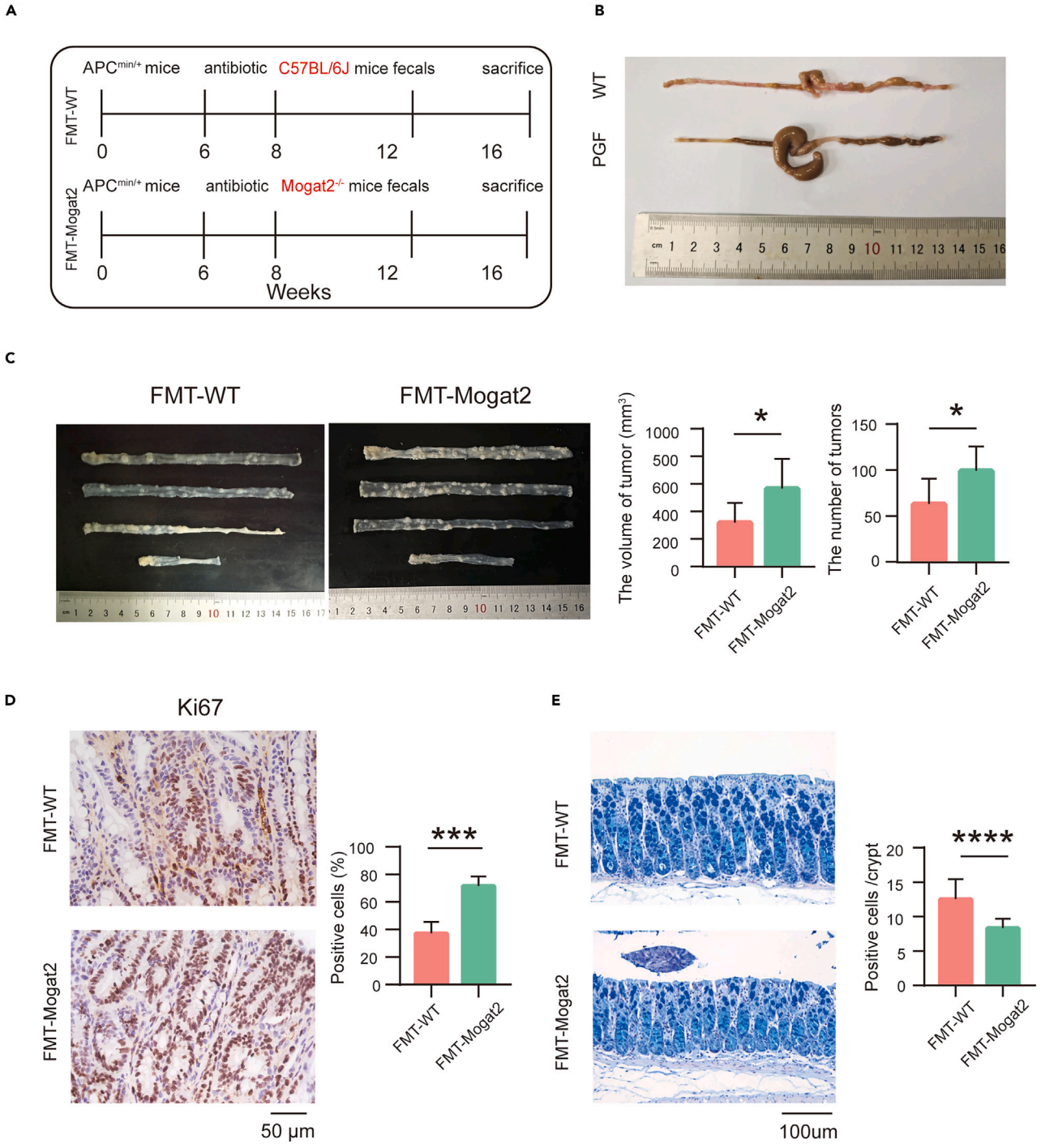

Figure 4. Gut microbiota from Mogat2$^{-/-}$ mice enhances the progression of intestinal adenoma in Apc$^{Min/+}$ mice

(A) An experimental design indicating the establishment process.

(B) Pseudo-germ-free mice developed caecal enlargement.

(C) The total number and volume of tumors in each group were calculated (n = 8).

(D) Immunohistochemical staining for Ki67 in the intestinal tumor tissues from FMT-WT mice and FMT-mogat2 mice was performed.

(E) The number of colon goblet cells was evaluated by AB-PAS staining. Significance was established by unpaired t test. (C, D, E). ****$p < 0.0001$, ***$p < 0.001$, *$p < 0.05$.

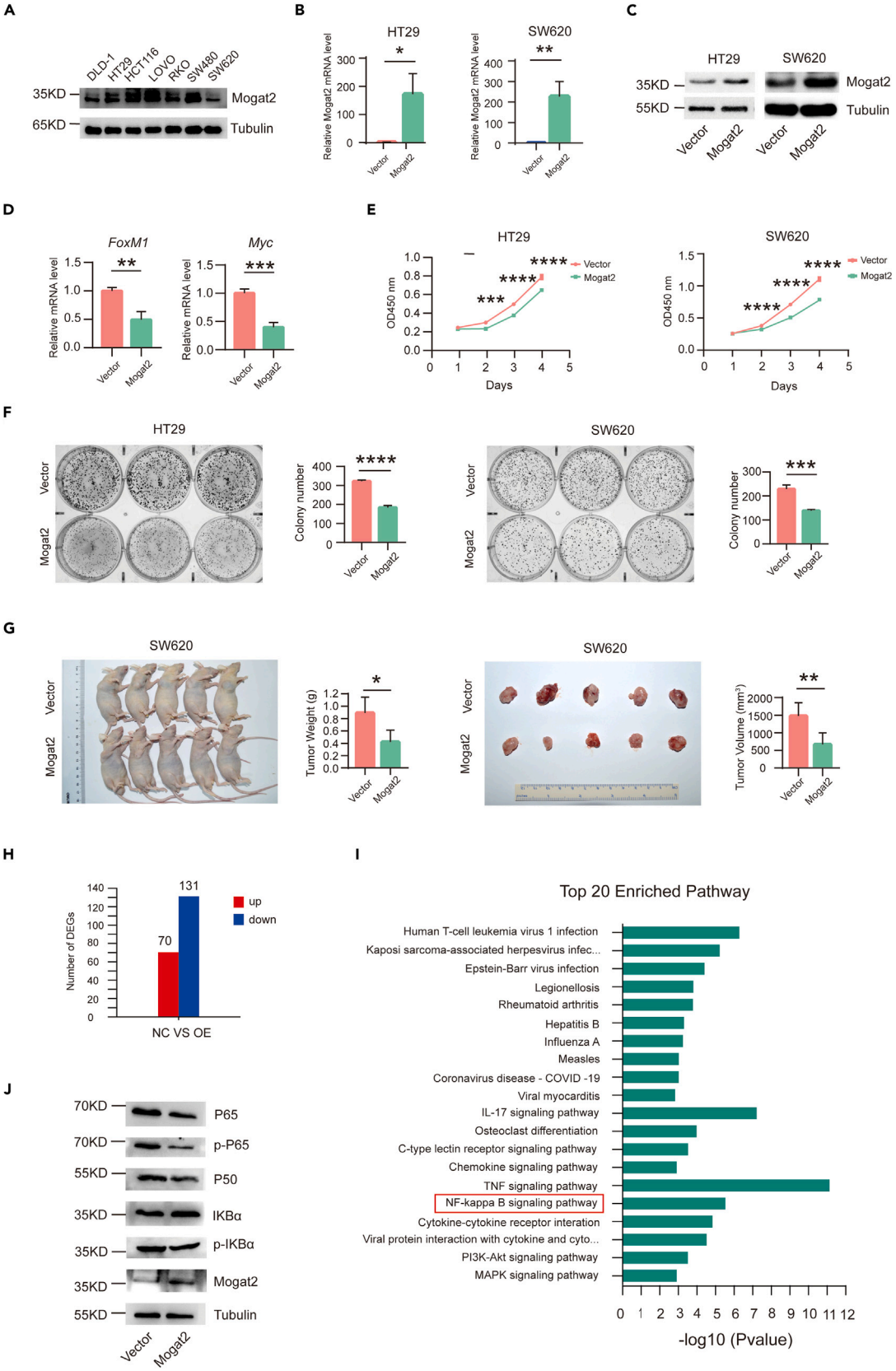
A
DLD-1
HT29
HCT116
LOVO
RKO
SW480
SW620
35KD
Mogat2
65KD
Tubulin
B
HT29
SW620
Relative Mogat2 mRNA level
Vector
Mogat2
C
HT29
SW620
35KD
55KD
Mogat2
Tubulin
Vector
Mogat2
D
FoxM1
Myc
Relative mRNA level
Vector
Mogat2
E
HT29
SW620
OD450 nm
Days
Vector
Mogat2
F
HT29
SW620
Vector
Mogat2
Colony number
G
SW620
SW620
Tumor Weight (g)
Tumor Volume (mm3)
H
Number of DEGs
up
down
70
131
NC VS OE
I
Top 20 Enriched Pathway
Human T-cell leukemia virus 1 infection
Kaposi sarcoma-associated herpesvirus infec...
Epstein-Barr virus infection
Legionellosis
Rheumatoid arthritis
Hepatitis B
Influenza A
Measles
Coronavirus disease - COVID -19
Viral myocarditis
IL-17 signaling pathway
Osteoclast differentiation
C-type lectin receptor signaling pathway
Chemokine signaling pathway
TNF signaling pathway
NF-kappa B signaling pathway
Cytokine-cytokine receptor interation
Viral protein interaction with cytokine and cyto...
PI3K-Akt signaling pathway
MAPK signaling pathway
-log10 (Pvalue)
J
70KD
P65
70KD
p-P65
55KD
P50
35KD
IKBα
35KD
p-IKBα
35KD
Mogat2
55KD
Tubulin
Vector
Mogat2

Figure 5. Over-expression of Mogat2 inhibits the proliferation of CRC cells

(A) The protein level of Mogat2 in CRC cells was measured.

(B and C) Quantitative PCR performed to detect Mogat2 mRNA expression in HT29 and SW620 cells. Mogat2 mRNA level was normalized to β-actin, Column, mean; bar, s.d. (from triplicates).

(D) The mRNA level of the proliferation genes FoxM1 and Myc were measured in SW620 cells upon Mogat2 overexpression, FoxM1 and Myc mRNA level was normalized to β-actin, Column, mean; bar, s.d. (from triplicates).

(E) The result of the CCK8 proliferation assay, Student's t test was used to perform the statistical analyses.

(F) The colony formation assay conducted in HT29 and SW620 cells upon Mogat2 overexpression, Student's t test was used to perform the statistical analyses.

(G) The xenograft tumor growth of SW620 cells was measured upon Mogat2 overexpression. *, $p < 0.05$, **, $p < 0.01$, and ****, $p < 0.0001$.

(H) Differentially expressed genes in Mogat2-overexpressing SW620 cells compared to Vector SW620 cells from the RNA-Sequencing (RNA-Seq) analysis.

(I) KEGG pathway enrichment analysis in CRC cells with Mogat2 overexpression.

(J) NF-κB signaling makers in Mogat2 overexpressing SW620 cells and SW620 Vector cells were evaluated by immunoblotting.

Ethics approval and consent to participate

The animal experiments were approved by the institutional ethics committee of Sun Yat-sen University, Guangzhou, China (Approval No: L102012016008E).

Availability of data and materials

Some of the clinical survival data can be found in the GEPIA database (http://gepia.cancer-pku.cn/). All the other data can be found in the article or the supplementary data.

Consent for publication

Not applicable.

Limitations of the study

Our data demonstrate that Mogat2 plays a tumor-suppressive role in the formation of intestinal tumors and that gut microbiota from Mogat2$^{-/-}$ mice aggravates the progression of intestinal adenoma. However, the study has several limitations. First, it is necessary to identify the specific strains and metabolites that facilitate adenoma progression. Second, while overexpression of Mogat2 in CRC cells appears to inhibit the NF-κB pathway, further research is required to understand how Mogat2 interacts with NF-κB signaling. Third, the detailed molecular mechanisms explaining how monoacylglycerol acyltransferase-2 suppresses colorectal cancer carcinogenesis in APC$^{min+/-}$ mice through the modulation of gut microbiota are yet to be elucidated.

STAR★METHODS

Detailed methods are provided in the online version of this paper and include the following:

- KEY RESOURCES TABLE
- RESOURCE AVAILABILITY
  - Lead contact
  - Materials availability
  - Data and code availability
- EXPERIMENTAL MODEL AND STUDY PARTICIPANT DETAILS
  - Animals
- METHOD DETAILS
  - Analysis of intestinal tumors
  - Orthotopic-transplantation model of mouse colon-cancer cell line MC38
  - Hematoxylin and Eosin (H&E) and Immunohistochemistry (IHC)
  - Enzyme-Linked Immunosorbent Assay (ELISA)
  - Immunoblotting
  - Stable overexpression of Mogat2 in HT29 and SW620 cells
  - Cell culture and reagents
  - Cell proliferation assay and colony formation assay
  - DNA extraction and polymerase chain reaction (PCR) amplification
  - Establishment of pseudo-germ-free (PGF) mouse model and FMT
- QUANTIFICATION AND STATISTICAL ANALYSIS

SUPPLEMENTAL INFORMATION

Supplemental information can be found online at https://doi.org/10.1016/j.isci.2024.110205.

ACKNOWLEDGMENTS

The authors would like to thank Exploring Health, LLC for their technical support. Schematic figure was drawn by Figdraw (www.figdraw.com). Funding: This work was supported by grants from the National Natural Science Foundation of China (No. 82073220, No. 82172815, No. 81902473, No. 81972301) and the Natural Science Foundation of Guangdong Province, China (No. 2024A1515012800).

AUTHOR CONTRIBUTIONS

C.N.Q. and J.L.Q. design, conceptualization, revision, and supervision. Y.H.L. experimental work and writing the original draft. C.R.Z., L.L.G., and Z.J.L. project administration. D.L.Z., X.C., and L.Y.D. data analysis and interpretation. Y. N. and B.J.H. writing and editing. C.N.Q., B.K.L., and Y.F.Y. funding acquisition.

DECLARATION OF INTERESTS

The authors declare that there are no conflicts of interest regarding the publication of this paper.

Received: September 24, 2023
Revised: April 18, 2024
Accepted: June 4, 2024
Published: June 6, 2024

REFERENCES

1. Wang, G., Fan, D., Gu, J., Ding, K., Fang, X., Shen, L., Xu, Z., Xu, J., Cai, J., Cai, L., et al. (2023). CACA guidelines for holistic integrative management of rectal cancer. Holist. Integr. Oncol. *2*, 1. https://doi.org/10.1007/s44178-023-00023-2.
2. Xie, S.-H., Huang, R.-Q., Liu, Y.-L., Cao, S.-M., and Qian, C.N. (2022). An increase in early cancer detection rates at a single cancer center: Experiences from Sun Yat-sen University Cancer Center. Vis. Cancer Med. *3*, 1. https://doi.org/10.1051/vcm/2022001.
3. Shailes, H., Tse, W.Y., Freitas, M.O., Silver, A., and Martin, S.A. (2022). Statin Treatment as a Targeted Therapy for APC-Mutated Colorectal Cancer. Front. Oncol. *12*, 880552. https://doi.org/10.3389/fonc.2022.880552.
4. Zhao, K., Jin, S., Wei, B., Cao, S., and Xiong, Z. (2018). Association study of genetic variation of lncRNA MALAT1 with carcinogenesis of colorectal cancer. Cancer Manag. Res. *10*, 6257–6261. https://doi.org/10.2147/CMAR.S177244.
5. Hull, M., and Lagergren, J. (2014). Obesity and colorectal cancer. Gut *63*, 205. https://doi.org/10.1136/gutjnl-2013-304988.
6. Pendyala, S., and Holt, P. (2008). Obesity and colorectal cancer risk. Gastroenterology *134*, 896. https://doi.org/10.1053/j.gastro.2008.01.024.
7. Ocvirk, S., and O'Keefe, S.J.D. (2021). Dietary fat, bile acid metabolism and colorectal cancer. Semin. Cancer Biol. *73*, 347–355. https://doi.org/10.1016/j.semcancer.2020.10.003.
8. Wan, Y., Wu, K., Wang, L., Yin, K., Song, M., Giovannucci, E.L., and Willett, W.C. (2022). Dietary fat and fatty acids in relation to risk of colorectal cancer. Eur. J. Nutr. *61*, 1863–1873. https://doi.org/10.1007/s00394-021-02777-9.
9. Hu, X., Fatima, S., Chen, M., Xu, K., Huang, C., Gong, R.H., Su, T., Wong, H.L.X., Bian, Z., and Kwan, H.Y. (2021). Toll-like receptor 4 is a master regulator for colorectal cancer growth under high-fat diet by programming cancer metabolism. Cell Death Dis. *12*, 791. https://doi.org/10.1038/s41419-021-04076-x.
10. Guo, H., Zhuang, K., Ding, N., Hua, R., Tang, H., Wu, Y., Yuan, Z., Li, T., and He, S. (2022). High-fat diet induced cyclophilin B enhances STAT3/lncRNA-PVT1 feedforward loop and promotes growth and metastasis in colorectal cancer. Cell Death Dis. *13*, 883. https://doi.org/10.1038/s41419-022-05328-0.
11. Loh, N.Y., Wang, W., Noordam, R., and Christodoulides, C. (2022). Obesity, Fat Distribution and Risk of Cancer in Women and Men: A Mendelian Randomisation Study. Nutrients *14*, 5259. https://doi.org/10.3390/nu14245259.
12. Long, M., Wang, W., and Sun, Q. (2020). A high-fat diet: an unexpected role in preventing the metastatic seeding of colorectal cancer. Signal Transduct. Targeted Ther. *5*, 257. https://doi.org/10.1038/s41392-020-00386-2.
13. Banh, T., Nelson, D.W., Gao, Y., Huang, T.N., Yen, M.I., and Yen, C.L.E. (2015). Adult-onset deficiency of acyl CoA:monoacylglycerol acyltransferase 2 protects mice from diet-induced obesity and glucose intolerance. J. Lipid Res. *56*, 379–389. https://doi.org/10.1194/jlr.M055228.
14. Bhatt-Wessel, B., Jordan, T.W., Miller, J.H., and Peng, L. (2018). Role of DGAT enzymes in triacylglycerol metabolism. Arch. Biochem. Biophys. *655*, 1–11. https://doi.org/10.1016/j.abb.2018.08.001.
15. Jin, Y., McFie, P.J., Banman, S.L., Brandt, C., and Stone, S.J. (2014). Diacylglycerol acyltransferase-2 (DGAT2) and monoacylglycerol acyltransferase-2 (MGAT2) interact to promote triacylglycerol synthesis. J. Biol. Chem. *289*, 28237–28248. https://doi.org/10.1074/jbc.M114.571190.
16. Mul, J.D., Begg, D.P., Haller, A.M., Pressler, J.W., Sorrell, J., Woods, S.C., Farese, R.V., Jr., Seeley, R.J., and Sandoval, D.A. (2014). MGAT2 deficiency and vertical sleeve gastrectomy have independent metabolic effects in the mouse. Am. J. Physiol. Endocrinol. Metab. *307*, E1065–E1072. https://doi.org/10.1152/ajpendo.00376.2014.
17. Nelson, D.W., Gao, Y., Yen, M.I., and Yen, C.L.E. (2014). Intestine-specific deletion of acyl-CoA:monoacylglycerol acyltransferase (MGAT) 2 protects mice from diet-induced obesity and glucose intolerance. J. Biol. Chem. *289*, 17338–17349. https://doi.org/10.1074/jbc.M114.555961.
18. Yen, C.L.E., Nelson, D.W., and Yen, M.I. (2015). Intestinal triacylglycerol synthesis in fat absorption and systemic energy metabolism. J. Lipid Res. *56*, 489–501. https://doi.org/10.1194/jlr.R052902.
19. Nelson, D.W., Gao, Y., Spencer, N.M., Banh, T., and Yen, C.L.E. (2011). Deficiency of MGAT2 increases energy expenditure without high-fat feeding and protects genetically obese mice from excessive weight gain. J. Lipid Res. *52*, 1723–1732. https://doi.org/10.1194/jlr.M016840.
20. Cao, J., Burn, P., and Shi, Y. (2003). Properties of the mouse intestinal acyl-CoA:monoacylglycerol acyltransferase, MGAT2. J. Biol. Chem. *278*, 25657–25663. https://doi.org/10.1074/jbc.M302835200.
21. Xiao, Y., Liu, Z., Liao, C., Mao, X., Cai, J., Xia, K., Qi, J., Huang, H., Yang, T., and Duan, Q. (2017). Inhibition of BET bromodomain improves anemia in APC(min) mice. Leuk. Lymphoma *58*, 989–992. https://doi.org/10.1080/10428194.2016.1219907.
22. Sui, Y., Hoshi, N., Ohgaki, R., Kong, L., Yoshida, R., Okamoto, N., Kinoshita, M., Miyazaki, H., Ku, Y., Tokunaga, E., et al. (2023). LAT1 expression influences Paneth cell number and tumor development in Apc(Min/+) mice. J. Gastroenterol. *58*, 444–457. https://doi.org/10.1007/s00535-023-01960-5.
23. Wang, L., and Zhang, Q. (2015). Application of the Apc(Min/+) mouse model for studying inflammation-associated intestinal tumor. Biomed. Pharmacother. *71*, 216–221. https://doi.org/10.1016/j.biopha.2015.02.023.
24. Kang, D.H., Lee, D.J., Lee, S., Lee, S.Y., Jun, Y., Kim, Y., Kim, Y., Lee, J.S., Lee, D.K., Lee, S., et al. (2017). Interaction of tankyrase and peroxiredoxin II is indispensable for the survival of colorectal cancer cells. Nat. Commun. *8*, 40. https://doi.org/10.1038/s41467-017-00054-0.
25. Li, J., Zhou, Z., Zhang, X., Zheng, L., He, D., Ye, Y., Zhang, Q.Q., Qi, C.L., He, X.D., Yu, C., et al. (2017). Inflammatory Molecule, *PSGL-1*, Deficiency Activates Macrophages to Promote Colorectal Cancer Growth through

NFκB Signaling. Mol. Cancer Res. *15*, 467–477. https://doi.org/10.1158/1541-7786.MCR-16-0309.

26. Li, L., Li, X., Zhong, W., Yang, M., Xu, M., Sun, Y., Ma, J., Liu, T., Song, X., Dong, W., et al. (2019). Gut microbiota from colorectal cancer patients enhances the progression of intestinal adenoma in Apc(min/+) mice. EBioMedicine *48*, 301–315. https://doi.org/10.1016/j.ebiom.2019.09.021.
27. Li, Y., Kundu, P., Seow, S.W., de Matos, C.T., Aronsson, L., Chin, K.C., Kärre, K., Pettersson, S., and Greicius, G. (2012). Gut microbiota accelerate tumor growth via c-jun and STAT3 phosphorylation in APCMin/+ mice. Carcinogenesis *33*, 1231–1238. https://doi.org/10.1093/carcin/bgs137.
28. Dai, Z., Zhang, J., Wu, Q., Chen, J., Liu, J., Wang, L., Chen, C., Xu, J., Zhang, H., Shi, C., et al. (2019). The role of microbiota in the development of colorectal cancer. Int. J. Cancer *145*, 2032–2041. https://doi.org/10.1002/ijc.32017.
29. Janney, A., Powrie, F., and Mann, E.H. (2020). Host-microbiota maladaptation in colorectal cancer. Nature *585*, 509–517. https://doi.org/10.1038/s41586-020-2729-3.
30. Wong, C.C., and Yu, J. (2023). Gut microbiota in colorectal cancer development and therapy. Nat. Rev. Clin. Oncol. *20*, 429–452. https://doi.org/10.1038/s41571-023-00766-x.
31. Kim, J., and Lee, H.K. (2021). Potential Role of the Gut Microbiome In Colorectal Cancer Progression. Front. Immunol. *12*, 807648. https://doi.org/10.3389/fimmu.2021.807648.
32. Fernandes, M.R., Aggarwal, P., Costa, R.G.F., Cole, A.M., and Trinchieri, G. (2022). Targeting the gut microbiota for cancer therapy. Nat. Rev. Cancer *22*, 703–722. https://doi.org/10.1038/s41568-022-00513-x.
33. Gong, Y., Dong, R., Gao, X., Li, J., Jiang, L., Zheng, J., Cui, S., Ying, M., Yang, B., Cao, J., and He, Q. (2019). Neohesperidin prevents colorectal tumorigenesis by altering the gut microbiota. Pharmacol. Res. *148*, 104460. https://doi.org/10.1016/j.phrs.2019.104460.
34. Garrett, W.S. (2015). Cancer and the microbiota. Science *348*, 80–86. https://doi.org/10.1126/science.aaa4972.
35. Peters, B.A., Dominianni, C., Shapiro, J.A., Church, T.R., Wu, J., Miller, G., Yuen, E., Freiman, H., Lustbader, I., Salik, J., et al. (2016). The gut microbiota in conventional and serrated precursors of colorectal cancer. Microbiome *4*, 69. https://doi.org/10.1186/s40168-016-0218-6.
36. Macchione, I.G., Lopetuso, L.R., Ianiro, G., Napoli, M., Gibiino, G., Rizzatti, G., Petito, V., Gasbarrini, A., and Scaldaferri, F. (2019). Akkermansia muciniphila: key player in metabolic and gastrointestinal disorders. Eur. Rev. Med. Pharmacol. Sci. *23*, 8075–8083. https://doi.org/10.26355/eurrev_201909_19024.
37. Zhang, T., Li, Q., Cheng, L., Buch, H., and Zhang, F. (2019). Akkermansia muciniphila is a promising probiotic. Microb. Biotechnol. *12*, 1109–1125. https://doi.org/10.1111/1751-7915.13410.
38. Cani, P.D., Depommier, C., Derrien, M., Everard, A., and de Vos, W.M. (2022). Akkermansia muciniphila: paradigm for next-generation beneficial microorganisms. Nat. Rev. Gastroenterol. Hepatol. *19*, 625–637. https://doi.org/10.1038/s41575-022-00631-9.
39. Yi, Z., Liu, X., Liang, L., Wang, G., Xiong, Z., Zhang, H., Song, X., Ai, L., and Xia, Y. (2021). Antrodin A from Antrodia camphorata modulates the gut microbiome and liver metabolome in mice exposed to acute alcohol intake. Food Funct. *12*, 2925–2937. https://doi.org/10.1039/d0fo03345f.
40. Qu, S., Zheng, Y., Huang, Y., Feng, Y., Xu, K., Zhang, W., Wang, Y., Nie, K., and Qin, M. (2023). Excessive consumption of mucin by over-colonized Akkermansia muciniphila promotes intestinal barrier damage during malignant intestinal environment. Front. Microbiol. *14*, 1111911. https://doi.org/10.3389/fmicb.2023.1111911.
41. Kobyliak, N., Falalyeyeva, T., Kyriachenko, Y., Tseyslyer, Y., Kovalchuk, O., Hadiliia, O., Eslami, M., Yousefi, B., Abenavoli, L., Fagoonee, S., and Pellicano, R. (2022). Akkermansia muciniphila as a novel powerful bacterial player in the treatment of metabolic disorders. Minerva Endocrinol. *47*, 242–252. https://doi.org/10.23736/S2724-6507.22.03752-6.
42. Martin, O.C.B., Lin, C., Naud, N., Tache, S., Raymond-Letron, I., Corpet, D.E., and Pierre, F.H. (2015). Antibiotic suppression of intestinal microbiota reduces heme-induced lipoperoxidation associated with colon carcinogenesis in rats. Nutr. Cancer *67*, 119–125. https://doi.org/10.1080/01635581.2015.976317.
43. Yu, H., Lin, L., Zhang, Z., Zhang, H., and Hu, H. (2020). Targeting NF-κB pathway for the therapy of diseases: mechanism and clinical study. Signal Transduct. Targeted Ther. *5*, 209. https://doi.org/10.1038/s41392-020-00312-6.
44. Vaiopoulos, A.G., Athanasoula, K.C., and Papavassiliou, A.G. (2013). NF-κB in colorectal cancer. J. Mol. Med. *91*, 1029–1037. https://doi.org/10.1007/s00109-013-1045-x.
45. Soleimani, A., Rahmani, F., Ferns, G.A., Ryzhikov, M., Avan, A., and Hassanian, S.M. (2020). Role of the NF-κB signaling pathway in the pathogenesis of colorectal cancer. Gene *726*, 144132. https://doi.org/10.1016/j.gene.2019.144132.
46. Yen, C.L.E., Cheong, M.L., Grueter, C., Zhou, P., Moriwaki, J., Wong, J.S., Hubbard, B., Marmor, S., and Farese, R.V., Jr. (2009). Deficiency of the intestinal enzyme acyl CoA:monoacylglycerol acyltransferase-2 protects mice from metabolic disorders induced by high-fat feeding. Nat. Med. *15*, 442–446. https://doi.org/10.1038/nm.1937.
47. Cao, J., Hawkins, E., Brozinick, J., Liu, X., Zhang, H., Burn, P., and Shi, Y. (2004). A predominant role of acyl-CoA:monoacylglycerol acyltransferase-2 in dietary fat absorption implicated by tissue distribution, subcellular localization, and up-regulation by high fat diet. J. Biol. Chem. *279*, 18878–18886. https://doi.org/10.1074/jbc.M313272200.
48. Yang, M., Zhang, X., Liu, Q., Niu, T., Jiang, L., Li, H., Kuang, J., Qi, C., Zhang, Q., He, X., et al. (2020). Knocking out matrix metalloproteinase 12 causes the accumulation of M2 macrophages in intestinal tumor microenvironment of mice. Cancer Immunol. Immunother. *69*, 1409–1421. https://doi.org/10.1007/s00262-020-02538-3.
49. Qi, C., Li, B., Guo, S., Wei, B., Shao, C., Li, J., Yang, Y., Zhang, Q., Li, J., He, X., et al. (2015). P-Selectin-Mediated Adhesion between Platelets and Tumor Cells Promotes Intestinal Tumorigenesis in Apc(Min/+) Mice. Int. J. Biol. Sci. *11*, 679–687. https://doi.org/10.7150/ijbs.11589.
50. Xu, H., Zhang, Y., Peña, M.M., Pirisi, L., and Creek, K.E. (2017). Six1 promotes colorectal cancer growth and metastasis by stimulating angiogenesis and recruiting tumor-associated macrophages. Carcinogenesis *38*, 281–292. https://doi.org/10.1093/carcin/bgw121.

STAR★METHODS

KEY RESOURCES TABLE

REAGENT or RESOURCE	SOURCE	IDENTIFIER
Antibodies		
Rabbit monoclonal anti-Ki67	Cell Signaling Technology	Cat# 12202; RRID: AB_2620142
Rabbit polyclonal anti-MGAT2	Abcam	Cat# ab228950; RRID: AB_3105860
Rabbit polyclonal anti- Alpha Tubulin	Proteintech	Cat# 11224-1-AP; RRID: AB_2210206
Rabbit monoclonal anti-P65	Cell Signaling Technology	Cat# 8242; RRID: AB_10859369
Rabbit monoclonal anti-Phospho-P65	Cell Signaling Technology	Cat#3033; RRID: AB_331284
Rabbit polyclonal anti- P105/P50	Cell Signaling Technology	Cat#3035; RRID: AB_330564
Rabbit monoclonal anti- IKBα	Cell Signaling Technology	Cat#4812; RRID: AB_10694416
Rabbit monoclonal anti- Phospho- IKBα	Cell Signaling Technology	Cat#2859; RRID: AB_561111
Chemicals, peptides, and recombinant proteins		
RPMI-1640 medium	Gibco	Cat#C11875500BT
Protease Inhibitor Cocktail	Sigma	Cat#ZH-P8340
Puromycin	Invitrogen	Cat#A1113802
Ampicillin	Macklin	Cat#A830931
Neomycin	Macklin	Cat#N799581
Metronidazole	Macklin	Cat#M813526
Vancomycin	Macklin	Cat#V871983
Critical commercial assays		
ELISA kit	Cloud-clone	Cat#MEB526Ge
BCA Protein Assay Kit	Thermo Scientific	Cat#23227
Lenti-Pac HIV Kit	GeneCopoeia	Cat#LT002
Cell Counting Kit-8	Abmole	Cat#M4839
Experimental models: Organisms/strains		
Mogat2 homozygous knockout mice	the Jackson Laboratory	Cat#011085; RRID: IMSR_JAX:011085
The $Apc^{min/+}$ mice	GemPharmatech	Cat#T001457; RRID: IMSR_GPT:T001457
Software and algorithms		
Adobe Illustrator	Adobe	https://www.adobe.com/
GraphPad Prism 8.4.2	GraphPad	https://www.graphpad.com/
ImageJ 1.53	ImageJ	https://fr.vessoft.com/software/windows/download/imagej

RESOURCE AVAILABILITY

Lead contact

Further information and requests for resources should be directed to and will be fulfilled by the lead contact, Dr. Jiliang Qiu (qiujl@sysucc.org.cn).

Materials availability

This study did not generate new unique reagents and all materials in this study are commercially available.

Data and code availability

- All data reported in this paper will be shared by the lead contact upon request.
- This paper does not report original code.
- Any additional information required to reanalyze the data reported in this paper is available from the lead contact upon request.

EXPERIMENTAL MODEL AND STUDY PARTICIPANT DETAILS

Animals

Mogat2 homozygous knockout mice were obtained from the Jackson Laboratory in Bar Harbor, USA, while the $Apc^{min/+}$ mice were obtained from GemPharmatech in Nanjing, China. All of the mice were in a C57BL/6J background. To generate $Apc^{min/+}$;$Mogat2^{+/-}$ mice, male $Apc^{min/+}$ mice were bred with female $Mogat2^{-/-}$ mice. Subsequently, the male $Apc^{min/+}$; $Mogat2^{+/-}$ mice were backcrossed with female $Mogat2^{-/-}$ mice to obtain $Apc^{Min/+}$; $Mogat2^{-/-}$ mice.[25,48] The mice were housed under specific pathogen-free conditions at the Animal Center of Guangdong Pharmaceutical University and all animal experiments were conducted with the approval of the Ethics Committee for Laboratory Animals of Sun Yat-sen University Cancer Center.

METHOD DETAILS

Analysis of intestinal tumors

Upon euthanizing and dissecting the mice, the colon and small intestines were carefully removed and opened longitudinally. Subsequently, the luminal contents were meticulously flushed with phosphate-buffered saline (PBS) solution and the small intestines divided into three equal segments: the proximal, middle and distal. The numbers and diameters of the tumors in the small intestines were measured using an inverted microscope. The small intestine tumor volumes were calculated using the formula: volume=$4/3\pi ab^2$ (where 'a' represents half of the long diameter and 'b' represents half of the short diameter).[25,49] The intestines were rolled with the mucosa facing outwards, fixed in 10% buffered formalin, processed and embedded in paraffin.

Orthotopic-transplantation model of mouse colon-cancer cell line MC38

The mouse colon-cancer cell line MC38 was grown in RPMI-1640 medium (Gibco) supplemented with 10% fetal bovine serum. Twelve 6-week-old male C57BL/6J mice were anesthetized with 5% isoflurane and then placed on a sterile heating pad. The abdomen, from which all hair was removed the previous day using depilatory cream, was prepared for sterile surgery by cleansing with ethanol and then betadine three times. A small midline abdominal incision was made using a scalpel to cut through the skin and scissors to carefully cut through the underlying musculature without damaging any organs. The cecum was exteriorized and placed on a piece of sterile gauze, then hydrated with sterile saline. Under microscopic guidance, a 100 μl suspension of 1×10^6 MC38 cells and Mogat2 overexpressed cells in PBS were carefully injected into the cecal wall. Afterwards, the cecum was then repositioned inside the peritoneum, and the muscle and skin incisions were closed with sutures.[50]

Hematoxylin and Eosin (H&E) and Immunohistochemistry (IHC)

Paraffin-embedded sections of intestines (4 μm in thickness) were stained with H&E and Alcian Blue Periodic Acid Schiff (AB-PAS) staining, following standard protocol.

For immunohistochemistry, the intestinal tissue slices were incubated with their corresponding primary antibodies. Specifically, anti-Ki67 (Cell Signaling Technology) was used at 1:200 dilution overnight at 4°C. The following day, the slices were treated with the secondary antibody for 30 minutes at 37°C, followed by DAB reaction and hematoxylin staining.

Enzyme-Linked Immunosorbent Assay (ELISA)

The serum level of Lipopolysaccharide (LPS) in the mice was measured using commercial ELISA kits (Cloud-clone) according to the manufacturer's instructions.

Immunoblotting

The cells were washed with cold PBS and lysed using a lysis buffer (Millipore) that was supplemented with a Protease Inhibitor Cocktail (Sigma) at 4°C for 20 minutes. The resulting lysates were centrifuged at 12000 rpm/min for 15 minutes at 4°C and the supernatants collected. Protein concentration was determined using the BCA Protein Assay Kit (Thermo Scientific). Afterwards, the protein was loaded onto an SDS-PAGE gel after boiling with a loading buffer at 99°C for 10 minutes, and then transferred onto a polyvinylidene difluoride (PVDF) membrane. The membrane was blocked with TBST containing 5% non-fat milk for 1 hour at room temperature, followed by overnight incubation with an MOGAT2 antibody (Abcam) at 4°C. Finally, the membrane was incubated with a secondary antibody for 1 hour at room temperature.

Stable overexpression of Mogat2 in HT29 and SW620 cells

Cell lines stably expressing either Mogat2 or the vector were constructed using pLVX-3X-Flag-Puro plasmids from the GeneCopoeia company. Lentiviruses for overexpression were produced in 293FT cells according to the procedure outlined in the Lenti-Pac HIV Kit (GeneCopoeia). Infectious lentiviruses were harvested 48 hours after transfection and filtered through a 0.45 mm filter (Millipore). Cells transduced with lentivirus were then cultured in 2 μg/mL of puromycin (Invitrogen) for two weeks to facilitate selection. The transfection efficiency was validated using Western Blot and qPCR, confirming the successful overexpression of Mogat2.

Cell culture and reagents

Colorectal carcinoma cell lines LOVO, RKO, DLD1, HT29, HCT-116, SW620, and SW480 were cultured in RPMI-1640 medium (Gibco) supplemented with 10% fetal bovine serum at 37°C in a humidified chamber containing 5% CO2.

Cell proliferation assay and colony formation assay

Cell proliferation was assessed using the Cell Counting Kit-8 (Abmole) according to the manufacturer's protocol. Specifically, 1×10^3 cells were seeded in 96-well plates, with each well containing 0.1 mL of medium. At designated time points (24, 48, 72, 96 hours), each well was incubated with 10 μL CCK8 solution for 2 hours at 37°C. Subsequently, an absorbance reading at 450 nm was taken using the Gen5 microplate reader (BioTek).

For the colony formation assay, a total of 2×10^3 cells were grown in each well of a 6-well plate and cultured for approximately 2 weeks. Afterwards, the cells were fixed with methanol for 30 minutes and subsequently stained with 2% crystal violet for 30 minutes. The number of colonies was then determined. These experiments were independently repeated three times.

DNA extraction and polymerase chain reaction (PCR) amplification

Fresh fecal samples were promptly collected and kept on ice before being stored at -80°C for subsequent use. The extracted DNA underwent evaluation on 1% agarose gel, and its concentration and purity were assessed using a NanoDrop 2000 UV-vis spectrophotometer (Thermo Scientific). The hypervariable region V3-V4 of the bacterial 16S rRNA gene was amplified with primer pairs 338F (5′-ACTCCTACGGGAGG CAGCAG-3′) and 806R (5′-GGACTACHVGGGTWTCTAAT-3′). The amplification process for the 16S rRNA gene involved initial denaturation at 95°C for 3 minutes, followed by 27 cycles of denaturation at 95°C for 30 seconds, annealing at 55°C for 30 seconds, and extension at 72°C for 45 seconds, with a final single extension step at 72°C for 10 minutes. The PCR procedure was carried out in triplicate. The PCR product was subsequently extracted from 2% agarose gel and purified using the AxyPrep DNA Gel Extraction Kit (Axygen Biosciences) according to manufacturer's instructions. The Quantus™ Fluorometer (Promega) was then used to quantify the resulting purified DNA.

Establishment of pseudo-germ-free (PGF) mouse model and FMT

$Apc^{min/+}$ mice at 6 weeks old were randomly divided into two groups. To induce a pseudo-germ-free state, their drinking water was supplemented with an antibiotic cocktail (1 g/L ampicillin, 1 g/L neomycin, and 1 g/L metronidazole, and 0.5 g/L vancomycin). All the antibiotics used were procured from Macklin in Shanghai, China.

Fresh fecal samples collected from WT mice (n=8) and $Mogat2^{-/-}$ mice (n=8) were then mixed at equal weights, respectively. The mixed feces were diluted in sterile PBS at a ratio of 1:10 (w/v), vigorously shaken for 3 minutes, and allowed to settle by gravity for 2 minutes. The mixture was then subjected to initial filtration, centrifugation, and homogenization. The resulting microbial suspensions were combined with 30% glycerol and stored at -80°C until used for gavage into $Apc^{Min/+}$ mice. For each gavage, 200 μL of the microbial suspension was administered to each mouse, and repeated twice a week over a 4-week period.

QUANTIFICATION AND STATISTICAL ANALYSIS

The results were analyzed using GraphPad Prism 8 and shown as mean ± SD from at least three independent experiments. The Kaplan-Meier method was used to calculate the survival curves, and the log-rank test was used to determine the statistical significance. Differences between groups were analyzed using two-tailed Student's t-tests and two-way analysis of variance (ANOVA). Data were considered statistically significant when $P < 0.05$.